Imaging spectroscopy algorithms for mapping canopy foliar chemical and morphological traits and their uncertainties

Aditya Singh,[1,3] Shawn P. Serbin,[1,4] Brenden E. McNeil,[2] Clayton C. Kingdon,[1] and Philip A. Townsend[1]

[1]*Department of Forest and Wildlife Ecology, University of Wisconsin, 1630 Linden Drive, Madison, Wisconsin 53706 USA*
[2]*Department of Geology and Geography, West Virginia University, Morgantown, West Virginia 26506 USA*

Abstract. A major goal of remote sensing is the development of generalizable algorithms to repeatedly and accurately map ecosystem properties across space and time. Imaging spectroscopy has great potential to map vegetation traits that cannot be retrieved from broadband spectral data, but rarely have such methods been tested across broad regions. Here we illustrate a general approach for estimating key foliar chemical and morphological traits through space and time using NASA's Airborne Visible/Infrared Imaging Spectrometer (AVIRIS-Classic). We apply partial least squares regression (PLSR) to data from 237 field plots within 51 images acquired between 2008 and 2011. Using a series of 500 randomized 50/50 subsets of the original data, we generated spatially explicit maps of seven traits (leaf mass per area (M_{area}), percentage nitrogen, carbon, fiber, lignin, and cellulose, and isotopic nitrogen concentration, $\delta^{15}N$) as well as pixel-wise uncertainties in their estimates based on error propagation in the analytical methods. Both M_{area} and %N PLSR models had a $R^2 > 0.85$. Root mean square errors (RMSEs) for both variables were less than 9% of the range of data. Fiber and lignin were predicted with $R^2 > 0.65$ and carbon and cellulose with $R^2 > 0.45$. Although R^2 of %C and cellulose were lower than M_{area} and %N, the measured variability of these constituents (especially %C) was also lower, and their RMSE values were beneath 12% of the range in overall variability. Model performance for $\delta^{15}N$ was the lowest ($R^2 = 0.48$, RMSE = 0.95‰), but within 15% of the observed range. The resulting maps of chemical and morphological traits, together with their overall uncertainties, represent a first-of-its-kind approach for examining the spatiotemporal patterns of forest functioning and nutrient cycling across a broad range of temperate and sub-boreal ecosystems. These results offer an alternative to categorical maps of functional or physiognomic types by providing non-discrete maps (i.e., on a continuum) of traits that define those functional types. A key contribution of this work is the ability to assign retrieval uncertainties by pixel, a requirement to enable assimilation of these data products into ecosystem modeling frameworks to constrain carbon and nutrient cycling projections.

Key words: AVIRIS, Airborne Visible/Infrared Imaging Spectrometer; carbon cycling; deciduous and coniferous forests; foliar traits; imaging spectroscopy; leaf chemistry; leaf morphology; nutrient cycling; PLS regression; spatial mapping; uncertainty.

Introduction

Terrestrial ecosystems play an important role in the global carbon cycle by sequestering 3–5 Pg of carbon (C) per year from the atmosphere via photosynthesis (see Schimel 1995, Cramer et al. 2001, 2007, Le Quere et al. 2009). Characterization of the factors that influence terrestrial C uptake is required to develop an improved process-based understanding of ecosystem dynamics and accurately model vegetation response to global change. However, there remains a large uncertainty in the

magnitude, seasonality, and location of this flux (Friedlingstein et al. 2014).

Chemical, structural, and morphological properties of the foliage in vegetation canopies correlate strongly with plant function, including ecosystem-wide nutrient cycling rates (Scott and Binkley 1997, Craine et al. 2002, Santiago et al. 2004, Meier and Bowman 2008) and photosynthetic capacity (Reich et al. 1997, 1999, Shipley et al. 2005, Kergoat et al. 2008). Thus, to map ecosystem productivity, modeling efforts to estimate the dynamics of global carbon stocks should make use of "functional biogeographic" (Violle et al. 2014) information on the covariance between plant traits and patterns of biogeochemical cycling (Enquist et al. 2007). The use of remote imaging spectroscopy to map key plant trait patterns—those that govern carbon and nutrient dynamics—will greatly enhance our understanding of ecosystem functioning (Ustin and Gamon 2010).

Global patterns of nutrient cycling and primary productivity in forested ecosystems are driven, in large part, by a tractable suite of foliar structural and biochemical traits representing a trade-off between leaf construction costs and photosynthetic carbon uptake potential (Reich et al. 1992, Shipley and Lechowicz 2000, Wright et al. 2004, Shipley et al. 2005, 2006). This defines a spectrum of plant function from slow-growing, nutrient-poor species to fast-growing, nutrient-rich, albeit "leaky," plants. Specifically, coordination between foliar nitrogen content and specific leaf area (SLA, or its reciprocal, leaf mass per area, M_{area}) maximizes C fixation (Shipley et al. 2005), with lower SLA resulting in lower foliage photosynthetic potential per unit dry mass (Niinemets 2001), but greater leaf structural strength and consequently longer leaf life spans (Wright and Westoby 2002, Wright et al. 2005a, Violle et al. 2009). These patterns have been found to be consistent among broadleaf, needleleaf, and herbaceous species (Reich et al. 1991, 1992, Grime 2006) and have been found to operate independently of growth form or phylogeny (Shipley et al. 2006). Foliar nitrogen content (i.e., nitrogen on scaled to an area basis, g/m^2) scales with the content of RuBisCo, the key protein responsible for the carboxylation of RuBP in the initial steps of CO_2 fixation (Long 1991, Collatz et al. 1992, Ainsworth and Rogers 2007). Thus, foliar nitrogen reflects a plant's investment in photosynthetic enzymes, structure, and light-harvesting complexes that modulate photosynthetic parameters such as the maximum rates of carboxylation (V_{cmax}) and electron transport (J_{max}) (Long 1991, Ripullone et al. 2003).

Foliar nitrogen concentration and M_{area}/SLA also covary strongly with decomposition and nitrogen mineralization rates across ecosystems (Chapin 2003, Kazakou et al. 2006, Quested et al. 2007, Santiago 2007). Decomposition releases plant nutrients and drives the largest flux of terrestrial C to the atmosphere (Meier and Bowman 2008), and rates of decomposition are positively correlated with nitrogen content of foliage and litter, SLA, and leaf water content (Bonan 1993, Hattenschwiler et al. 2005, Fortunel et al. 2009) and negatively with leaf dry matter content (Quested et al. 2007, Fortunel et al. 2009, Kazakou et al. 2009) and foliar lignin concentrations (Hobbie et al. 2007, Johnson et al. 2007, Carrera and Bertiller 2010). Foliar lignin-to-nitrogen ratios are thus strong indicators of litter quality and consistent predictors of litter decomposability (Melillo et al. 1982, Knorr et al. 2005, Fortunel et al. 2009) and, together with cellulose concentration, regulate rates of late-stage forest litter decomposition (McClaugherty and Berg 1987, Berg 2000, Johnson et al. 2007).

Foliar isotopic N concentration ($\delta^{15}N$) is an integrator of the nitrogen cycle (Robinson 2001, Amundson et al. 2003) and has been used as an indicator of relative N availability to plants and a basis to infer N cycling rates (Austin and Vitousek 1998, Martinelli et al. 1999, Craine et al. 2009). Specifically, variations in N fractionation in foliar matter can indicate effects of climate on organic/inorganic nitrogen availability (Amundson et al. 2003, Craine et al. 2009) or local-scale variations in plant dependence on mycorrhizal associations (Hogberg 1997, Hobbie et al. 2000, Lilleskov et al. 2002, Craine et al. 2009). Spatial patterns of foliar isotopic N concentrations are also associated with plant response to disturbances (Amundson et al. 2003, McLauchlan et al. 2007) or elevated external inputs such as N deposition (Hogberg 1997, Emmett et al. 1998, McLauchlan et al. 2007).

Synoptic, repeatable, and consistent retrievals of key foliar traits such as foliar nitrogen, SLA (or M_{area}), foliar lignin and cellulose, and isotopic nitrogen are invaluable for characterizing determinants of ecosystem function across large regions (Chapin et al. 1996, Diaz et al. 2004, Ustin and Gamon 2010), and may provide valuable inputs for modeling nutrient fluxes and vegetation range shifts under changing land use and climate scenarios (Wright et al. 2004, Townsend et al. 2008). Remote sensing, specifically imaging spectroscopy, offers the capacity to map the primary drivers of plant trait variability from the landscape to the global scale (Ustin and Gamon 2010). Imaging spectrometers measure reflected light in narrow, contiguous wavebands (typically $\leq$10–15 nm) over a large portion of the incident solar spectrum (e.g., 350–2500 nm for NASA's Airborne Visible/Infrared Imaging Spectrometer, AVIRIS; see Vane et al. 1993, Green et al. 1998). It has long been demonstrated that reflectance spectroscopy is sensitive to foliar chemistry as well as the structural and morphological characteristics of plant canopies, and indeed, this is the basis for standard spectroscopic approaches to estimate chemistry on dried samples (Kokaly 2001, Richardson and Reeves 2005, Petisco et al. 2006) as well as to nondestructively estimate chemistry or photosynthetic properties of fresh leaves (Curran et al. 1992, Sims and Gamon 2002, Blackburn 2007, Menesatti et al. 2010). The ability to do this is a consequence of well-known biochemical absorption features at different wavelengths (Curran 1989, Curran et al. 1992, Fourty et al. 1996, Curran et al. 2001) related to electron transitions and bending and stretching of chemical bonds (Curran 1989, Fourty et al. 1996).

The ability to retrieve chemistry from remotely sensed imagery is complicated by a number of factors, including crown architecture and seasonality, although it is clear that chemical features related to leaf chlorophyll (Curran et al. 1992, Yoder and Pettigrewcrosby 1995, Curran et al. 2001) and water content are clearly expressed in both narrowband and broadband imagery (Gates et al. 1965, Tucker 1980, Asner and Vitousek 2005, Sanchez-Azofeifa et al. 2009, Ustin et al. 2012). The effects of canopy structure on reflectance may confound the identification of absorption features in foliage (Knyazikhin et al. 2013), for example, in wavelengths with high leaf scattering, but there is also

strong evidence that features identifiable at the leaf level can be detected in measurements at the canopy level (Baret et al. 1994). Ultimately, the coordination of traits at both the leaf and canopy level facilitates using spectral information to map traits of interest, even if the biophysical drivers of strong correlations at some wavelengths have not yet been fully characterized (Townsend et al. 2003, Ollinger 2011, Ollinger et al. 2013).

An extensive body of literature has demonstrated the capacity of imaging spectroscopy to map foliar traits relevant to photosynthesis (Wessman et al. 1989, Matson et al. 1994, Curran et al. 1997, Martin and Aber 1997, Coops et al. 2003, Smith et al. 2003, Townsend et al. 2003, Asner and Martin 2008, Martin et al. 2008, McNeil et al. 2008, Kokaly et al. 2009). In particular, spectra in the shortwave infrared (especially 1400–1850 nm and 2000–2400 nm) are critical to retrieval of parameters related to photosynthesis on account of strong absorption features related to nitrogen bonds in proteins that are expressed in those regions (Fourty et al. 1996). Studies also show that radiative transfer models (Asner 1998, Asner et al. 2008, 2011a, Asner and Martin 2008, 2009) can be used in conjunction with imaging spectroscopy to effectively map foliar traits. In general, existing efforts have been site specific (Martin and Aber 1997, Ollinger et al. 2002, Coops et al. 2003, Townsend et al. 2003) and, apart from Martin et al. (2008), studies that incorporate information from multiple scenes across multiple locations are rare (Appendix: Table A1). Here, we report a set of generalizable spectroscopic calibrations for the determination of leaf chemical composition (nitrogen, carbon, and fiber constituents), morphology (leaf mass per area, M_{area}), and isotopic composition ($\delta^{15}N$) of temperate and boreal tree species using imaging spectroscopy. Moreover, by demonstrating techniques to explicitly propagate uncertainties from the leaf to stand to image level, we show how our algorithms can be directly integrated into global change models that require uncertainty estimates of input parameters.

Materials and Methods

Study sites

We established 237 plots across a broad swath of the Upper Midwest and Northeast USA (Fig. 1). These plots sampled a range of broadleaf and needleleaf forests, including 36 dominant species (see Appendix: Table A2) reported by Serbin et al. (2014). Each plot consisted of two crossing 60 × 60 m transects, defining five points at which a metric factor-2 prism was used to tally trees by species (Townsend et al. 2003). Foliar biomass by species was estimated from diameter–biomass relationships in Jenkins et al. (2003), and was subsequently used to scale foliar trait estimates by species to the canopy of the entire plot.

We collected foliage from the top, middle, and bottom of the canopy of the predominant species on each plot (>5% of relative biomass) using a shotgun, line launcher, or pole pruner Plot-level values for each trait were estimated from the relative proportion of foliar biomass by species on a plot. We measured leaf-level percentage nitrogen (%N), carbon (%C), fiber (ADF), lignin (ADL), and cellulose, isotopic $^{15}N{:}^{14}N$ ratio ($\delta^{15}N$), and leaf mass per area (M_{area}), as well as their uncertainties, by species and by plot from reflectance spectroscopy on both dry and fresh samples (Serbin et al. 2014). Leaf-level trait measurements employed chemometric partial least-squares regression (PLSR) models that link contact reflectance spectra and measurements made using standard laboratory techniques. This approach facilitated estimation of per sample (i.e., per leaf) uncertainties of trait estimates. We scaled measurement uncertainty from leaf-level traits to estimates of canopy traits based on proportional foliar biomass. Leaf-to-canopy trait scaling used 1000 replicates drawn from the distributions of leaf-level estimates and their uncertainties from Serbin et al. (2014) to generate plot-level trait estimates and uncertainties. Note that we had trait estimates for multiple levels of the canopy at each plot, which facilitated testing the ability to map "whole-canopy" trait characteristics (see Ollinger et al. 2002) vs. top-of-canopy traits (presumably all that is visible to the sensor). Using data from Green et al. (2003) on vertical variation in foliar traits within a canopy profile, we weighed plot-level estimates according to four different schemes: (1) top weighted, 90% weight for top-of-canopy foliage, 9% weight for mid-canopy foliage, and 1% weight for bottom-canopy foliage; (2) top-to-middle weighted, 64.5%, 32.3%, and 3.2% weights for top, middle, and bottom canopy foliage; (3) whole canopy, 40%, 40%, and 20% weights for top, middle, and bottom canopy foliage; and (4) top only, where only the top-of-canopy foliage was considered (100% for top-of-canopy). We report results from top weighted scaling (option 1), but results and coefficients for the rest of the scaling options are provided in the Appendix and Supplement). For each of these options, uncertainty in relative foliar biomass was incorporated by randomly varying species-level biomass estimates by ±25% in each of the 1000 permutations. The Supplement provides plot locations, plot-level canopy trait estimates, and associated uncertainties.

Image processing

145 AVIRIS-Classic images were acquired from NASA's ER-2 platform during the summers of 2008–2011 at flight altitudes ranging from 14 000–20 000 m (pixel sizes of 12–18 m; see Fig. 1). Data were provided by the Jet Propulsion Laboratory as orthorectified, calibrated radiance images (Vane et al. 1993, Green et al. 1998), and all images were processed using a common processing stream to ensure comparability. We atmospherically corrected images using ATREM (TAFKAA algorithm; Gao et al. 2000, Montes and Gao 2004). Images were topographically corrected using the mod-
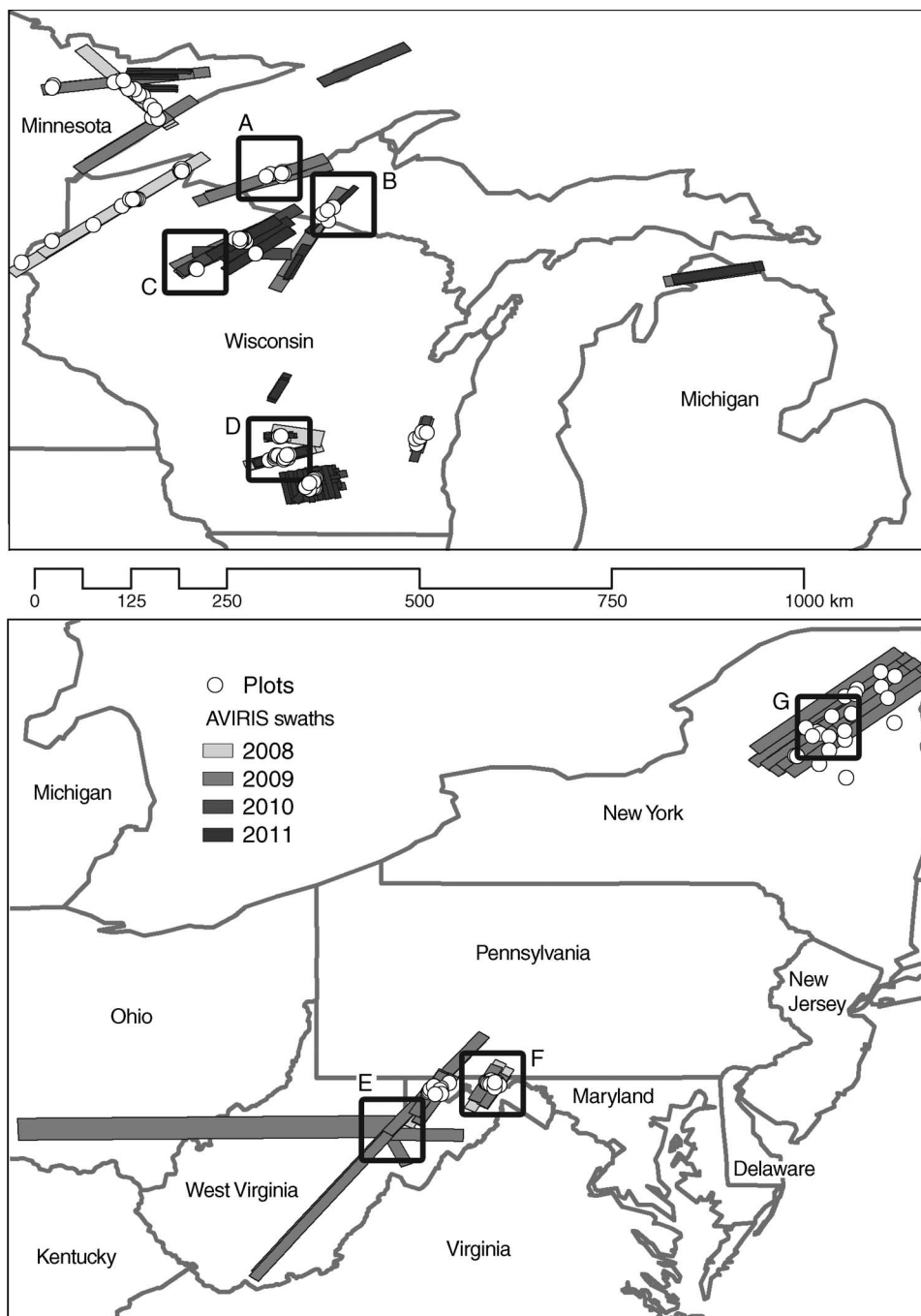
Fig. 1.   Locations of field sampling plots (237) overlaid on AVIRIS (NASA's Airborne Visible/Infrared Imaging Spectrometer) acquisitions (143) from 2008–2011 across a portion of the United States. Boxes indicate locations of sites graphed in subsequent figures; A, Porcupine Mountains State Forest, Michigan; B, Ottawa National Forest, Michigan; C, Flambeau River State Forest, Wisconsin; D, Devil's Lake State Park, Wisconsin; E, Fernow Experimental Forest, West Virginia; F, Green River State Forest, Maryland; G, Adirondack Park, New York.

ified sun-canopy-sensor topographic method (Soenen et al. 2005) and were BRDF (bidirectional reflectance distribution function; i.e., cross-track)-corrected using a quadratic function of the volumetric scattering term of the Ross-Thick BRDF model (Roujean et al. 1992,

Lucht et al. 2000). Post hoc georectification was performed on a small number of misaligned images, with final pixel registration errors < 0.5 pixel across all scenes. We used 51 images for model development and the remainder for testing and analysis.
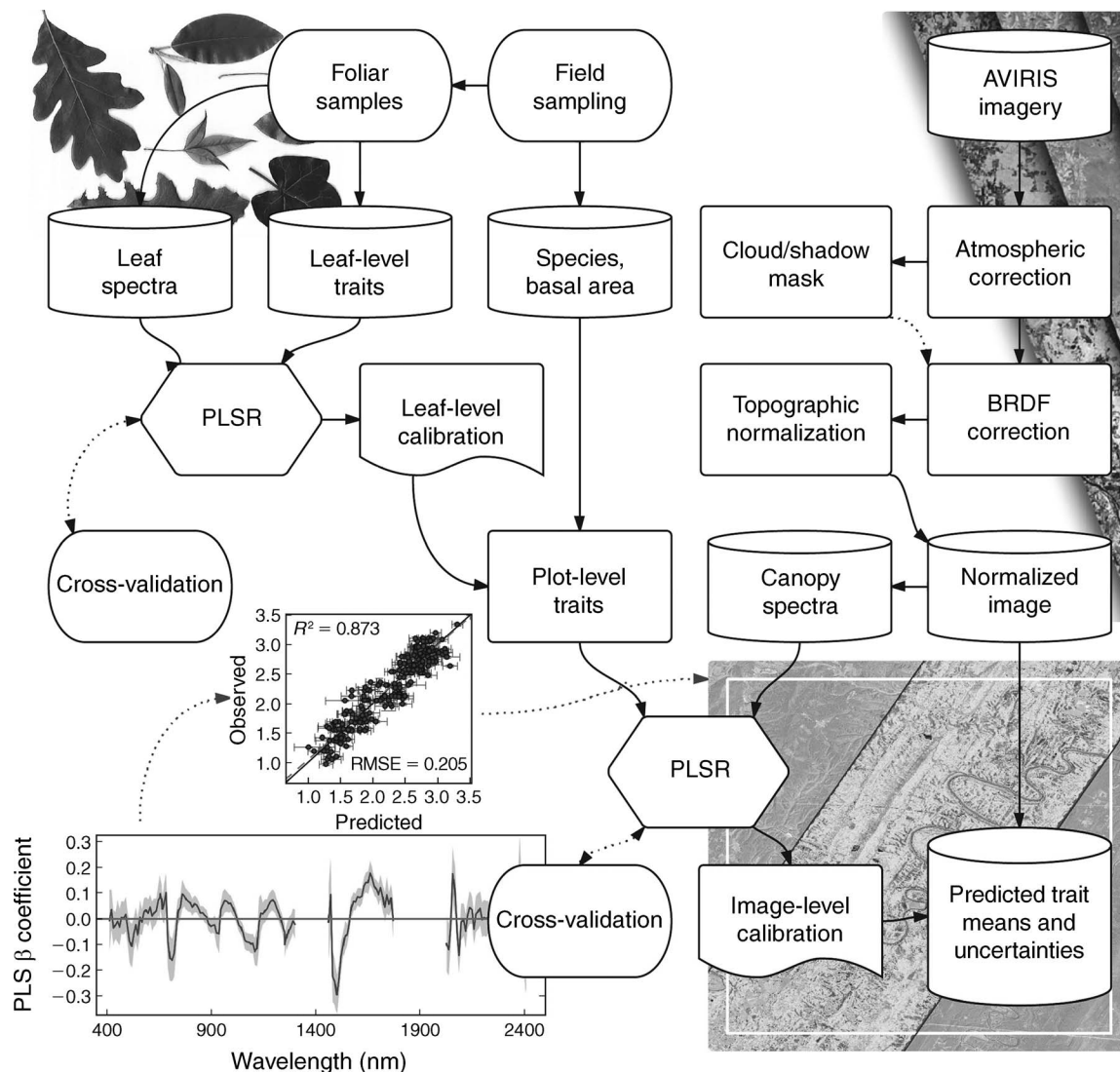
FIG. 2. Scaling leaf-level functional traits to the canopy using AVIRIS imagery. Abbreviations are: PLSR, partial least squares regression; BRDF, bidirectional reflectance distribution function. In the wavelength graph, the PLS β coefficient represents the standardized coefficient.

Statistical analysis

The general approach to the estimation of canopy traits (including chemistry) from imaging spectroscopy (IS) is illustrated in Fig. 2. We build upon the approach taken by Martin et al. (2008), in which they used data from eight study sites and 137 field plots to develop a general, cross-scene predictive equation for foliar nitrogen. We extend their effort by additionally deriving maps of carbon, leaf mass per area (M_{area}), fiber, lignin, and cellulose, as well as mapping uncertainties in all traits of interest. For each trait, we developed models using 500 permutations of our data, drawing randomly from the plot-level trait estimates and perturbing those estimates based on uncertainties propagated at every level of measurement (spectra, trait, foliar biomass, etc.).

For each of the 500 permutations, we randomly split our data 50/50 for calibration and validation. Because spectra for a given plot could have been sourced from multiple images available for each location, we further constrained the selection such that an observation could appear only once in the training set (i.e., training spectra for each plot came from a single image). This procedure was repeated 500 times and model coefficients, model fits, and predictions were saved for all iterations. We subsequently applied the 500 models to each pixel in all images. This allowed us to report the range of expected model performance and to calculate pixel-by-pixel uncertainty for the mapped models as the standard deviation of model predictions for all 500 permutations. To test if our models were stable across space and time,

TABLE 1. Summary statistics for canopy-level nutritional and morphological traits examined in this study, with means, standard deviations, and ranges of canopy foliar traits aggregated across 237 plots sampled from 2008–2011.

Trait	Overall Mean (SD)	Overall Range	Needleleaf Mean (SD)	Needleleaf Range	Broadleaf Mean (SD)	Broadleaf Range
M_{area} (g/m^2)	116.23 (44.81)	51.88–313.44	168.33 (29.00)	101.24–313.44	86.90 (16.47)	51.88–151.55
N (%)	2.20 (0.58)	0.96–3.31	1.60 (0.30)	0.96–2.48	2.54 (0.39)	1.20–3.31
C (%)	49.83 (1.14)	46.39–53.86	50.76 (0.77)	48.70–53.86	49.31 (0.97)	46.39–51.83
ADF (%)	37.49 (7.27)	18.02–53.04	44.48 (4.53)	35.10–53.04	33.55 (5.29)	18.02–48.31
ADL (%)	21.95 (4.72)	8.27–36.76	26.16 (2.71)	20.22–8.27	19.58 (3.88)	8.27–30.34
Cellulose (%)	16.06 (2.69)	8.66–23.42	17.92 (2.33)	11.60–23.42	15.02 (2.29)	8.66–22.22
δ^{15}N (‰)	−3.09 (1.68)	−7.98 to 0.41	−2.55 (1.97)	−7.75 to 0.41	−3.39 (1.41)	−7.98 to −0.53

Notes: Sampled plots across a large portion of the USA are shown in Fig. 1. Trait abbreviations are M_{area}, leaf mass per area; ADF, acid detergent fiber; ADL, acid detergent lignin. For leaf-level summaries, see Serbin et al. (2014).

we conducted additional cross-validations by reformulating PLSR models by leaving out data from individual geographic locations (areas with groups of plots; Fig. 1), or from years of image acquisition and evaluating model fits on the withheld data.

We employed partial least-squares regression, PLSR (Wold et al. 1984, Geladi and Kowalski 1986, Wolter et al. 2008), to predict canopy traits from imaging spectroscopy, as done in many previous studies (Coops et al. 2003, Smith et al. 2003, Townsend et al. 2003, Martin et al. 2008, McNeil et al. 2008, Deel et al. 2012). In practice, PLSR iteratively transforms predictor and response variables to find latent vectors and subsequently produce calibration factors and a linear model. PLS techniques achieve computational efficiency by maximizing the covariance between independent and dependent variables while simultaneously maintaining the constraint of being orthogonal to the previously determined factors (Wold et al. 1984, Geladi and Kowalski 1986, Frank and Friedman 1993, Wold et al. 2001). PLSR is better suited than traditional multiple linear regression methods for handling multi-collinear and over-sampled data, i.e., when the number of independent variables approaches or exceeds the number of observations (Wold et al. 1984, 2001, Geladi and Kowalski 1986). In particular, variations of unconstrained linear models (such as stepwise variable selection approaches; see Appendix: Table A1), violate cardinal assumptions of independent predictors and uncorrelated errors. At best, this results in biased estimates of beta coefficients (Tibshirani 1996) and underestimated errors and P values (Altman and Andersen 1989). Specific to chemometric data, stepwise selection procedures have been shown to perform poorly in calibration experiments (see Grossman et al. 1996) and may not generate results based on known absorption characteristics of materials being examined (Townsend et al. 2003). PLSR avoids difficulties in interpretation of synthetic PCA variables or the potential for modeling spurious relationships using stepwise regression (Grossman et al. 1996). The Predicted REsidual Sum of Squares (PRESS) statistic was used to select the appropriate number of PLS model components (Chen et al. 2004). We used the Variable Importance of Projection (VIP) statistic (Wold 1994) and standardized coefficient, by waveband,

to evaluate the contribution of each wavelength and associated absorption features to trait predictions. The VIP score reflects each predictor's (i.e., waveband) influence in fitting the PLSR model. It is based on the predictor's absolute coefficient size and partial R^2 within the overall PLSR model. Standardized coefficients are employed for graphing to account for scale differences in reflectance between different wavelength regions (i.e., higher reflectance and greater variability in the NIR equate to smaller coefficients, but not necessarily less important coefficients), as well as in the dependent variables (traits).

We averaged the 3×3 image pixel array surrounding each field plot's center, leaving us with one composite AVIRIS spectrum per 60×60 m plot. We postulate that averaging surrounding pixels is desirable because field plots in closed-canopy forests can rarely be identified to a specific pixel.

Finally, maps of the traits and their uncertainties were made for all AVIRIS images as the mean and standard deviation of the 500 permutations. Geographic patterns of trait distribution were analyzed with respect to gradients of latitude, precipitation, and temperature (derived from PRISM 2004), and nitrogen deposition (from NADP 2014).

RESULTS

Geographic variation in foliar traits

Canopy-averaged ranges of plot-level trait estimates stratified by leaf physiognomy are presented in Table 1 (data on plot-level foliar traits by species are in the Appendix: Table A2; the entire data set is in the Supplement). There was a nearly twofold difference in M_{area} between needleleaf and broadleaf species ($T = 28.88$, $P < 0.0001$), and mass-based nitrogen content of broadleaf species was around 1.5 times that of needleleaf species ($T = 24.15$, $P < 0.0001$). Carbon content, fiber, lignin, and cellulose exhibited less variation between needleleaf and broadleaf species, but all differences were significant ($P < 0.0001$). Deciduous-dominated plots showed slightly higher isotopic N content than coniferous-dominated plots ($T = 2.32$, $P = 0.02$). Correlation analyses revealed a strong negative relationship between leaf nitrogen and M_{area} ($r = -0.766$, $P < 0.0001$) as well

ADITYA SINGH ET AL.

TABLE 2. Pearson product moment correlation coefficients (r) between plot-level traits, latitude, mean annual precipitation (MAP), mean annual temperature (MAT), latitude (Lat.), and NADP total annual N deposition (N dep.).

Trait	N	M_{area}	C	ADF	ADL	Cellulose	$\delta^{15}N$	Lat.	MAT	MAP
M_{area}	−0.766 ****									
C	−0.618 ****	0.607 ****								
ADF	−0.624 ****	0.700 *****	0.623 ****							
ADL	−0.492 ****	0.649 ****	0.628 ****	0.931 ****						
Cellulose	−0.476 ****	0.501 ****	0.386 ****	0.865 ****	0.746 ****					
$\delta^{15}N$	0.108	0.211 **	0.005	−0.058	0.119	−0.226 **				
Lat.	−0.312 ****	0.307 ****	0.106	0.170 **	0.119	0.237 **	−0.177 **			
MAT	0.414 ****	−0.238 **	−0.219 **	−0.260 ****	−0.172 **	−0.282 ****	0.413 ****	−0.862 ****		
MAP	−0.135 *	−0.193 **	0.203 **	0.163 **	0.087	0.088	−0.455 ****	−0.352 ****	−0.134 *	
N dep.	0.392 ****	−0.066	−0.278 ****	−0.165 **	−0.121	−0.146 *	0.398 ****	0.021	0.205 **	−402 ****

Note: The NADP data source is http://nadp.sws.uiuc.edu/
* $P < 0.05$; ** $P < 0.01$; **** $P < 0.0001$.

as significant negative relationships with other leaf structural compounds (Table 2). Leaf nitrogen content decreased with latitude, while M_{area} increased, a reflection of an increasing dominance of needleleaf species in the north. We also found a significant positive correlation between foliar nitrogen and patterns of nitrogen deposition across our sites ($r = 0.392$, $P < 0.0001$). To further explore this relationship, we fit a mixed-effects model to predict foliar nitrogen concentrations while controlling for latitude with Gaussian random effects specified for species (not shown). The model explained 88.7% of the variation in foliar nitrogen, of which 59% was attributed to differences between species alone. The effects of elevated foliar nitrogen concentrations corresponding to the N deposition gradient were apparent ($P < 0.0001$), even after taking into consideration latitudinal gradients and

inherent differences between species. Foliar $\delta^{15}N$ concentrations were highly correlated with mean annual temperature and declined with mean annual precipitation (MAT, $r = 0.413$; MAP, $r = -0.455$; both $P < 0.0001$). We also found evidence of foliar isotopic N enrichment along the N deposition gradient ($r = 0.398$, $P < 0.0001$).

Canopy spectra

Canopy spectra were highly variable (Fig. 3), with nearly complete separation (± 1 SD) between spectra of all broadleaf and all needleleaf plots in the NIR (700–1400 nm) and the 1400–1900 nm SWIR1 regions. Spectra of the two physiognomic types partially overlapped in the visible (400–700 nm) and SWIR2 (1900–2400 nm) wavelengths. The highest spectral variability (in terms of the coefficient of variation; data
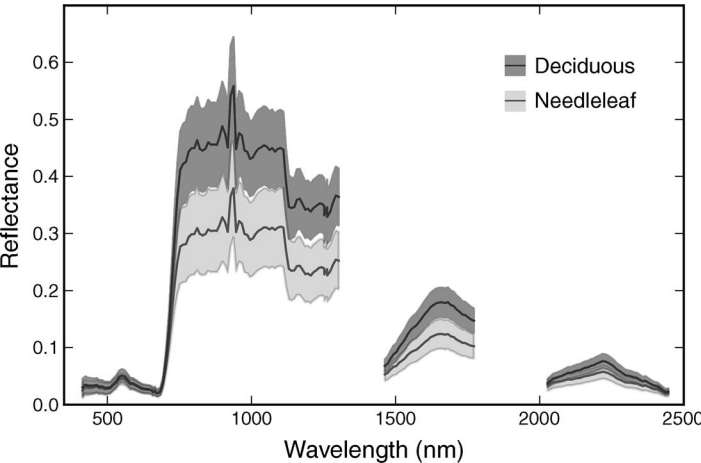

FIG. 3. Means (with standard deviation bands) of AVIRIS spectra obtained from 51 images and 237 plots stratified by dominant leaf habit (deciduous, needleleaf).

not shown) was observed in the visible regions of the spectrum (>23–50%) and was generally constant across the rest of the spectrum (~22%). Across all plots, needleleaf-dominated plots had ~10% less spectral variability than plots dominated by broadleaf species.

PLSR model results

Results for models built using the four aggregation schemes (Appendix: Table A3) were highly consistent. We provide model comparisons (Appendix: Figs. A1–A5) and PLSR coefficients from all canopy aggregation schemes and randomized models (Supplement), but focus here on results obtained using the top-weighted scheme. In our results, we show the model predictions from AVIRIS vs. field-based measurements (Fig. 4). Note that we show error bars in both directions: error on the y-axis is due to uncertainty of trait values from the scaling from leaf-level spectra to plot-level traits, whereas uncertainty on the x-axis is due to uncertainty from the image-based PLSR model. To our knowledge, this is the first time both uncertainties in the training data and mapped estimates have been provided. We also show standardized coefficients (Fig. 5), to compare wavebands important for mapping different traits. The shaded uncertainties in the standardized coefficients are based on the 500 permutations of the data used to generate the final maps. Additional diagnostics, such as VIP by wavelength and PRESS statistic by number of PLS coefficients (used to select the number coefficients in the PLS model), are graphed in Fig. 6. The Supplement lists the 500 raw PLS coefficients for the traits reported in this paper. These are the values that should be applied to make maps from new images that have been processed consistent with this study. We also show wavelength regions that correspond to known absorption features (from Curran 1989, Fourty et al. 1996, Curran et al. 2001). The standardized coefficients for mapping all of the traits from AVIRIS-Classic (except isotopic N, which has not previously been studied in depth) align in at least some wavelengths with known absorption features (Fig. 5; dotted bars).

Both M_{area} and %N had model fits with $R^2 > 0.85$, which are comparabe to the results reported by Martin et al. (2008); see Appendix: Table A2). Root mean square errors (RMSEs) for both variables were less than 9% of the range of data (Table 3). There was considerable spatial variation in retrieval uncertainties for both traits. High uncertainties (e.g., >2% for nitrogen or >10% for M_{area}) typically occurred at forest edges, in regions that were probably disturbed and where the dominant species were not represented in our database (e.g., crops or grasses and forbs in recently disturbed areas.). Fiber and lignin were predicted with $R^2 > 0.60$, and carbon and cellulose with $R^2 \sim 0.5$. Although R^2 values of fiber and lignin were lower than those of M_{area} and %N, their RMSE values were within 10% of the range of data. The comparatively lower R^2 values for %C and cellulose are related to the low

amount of natural variability in these constituents. Isotopic $\delta^{15}N$ had the worst fit of all models ($R^2 = 0.48$), but the RMSE was within 15% of the range in the data. Cross-validations conducted to test model stability across years and sites were in agreement with overall model results. Averaged across all strata (by year or by geographic area) and traits, more than 90% of held-out samples were predicted within the prediction error bounds of calibration models. In addition, validation errors of prediction (RMSEs) were well within the observed range of modeled traits, i.e., with RMSE values lower than 15% of the range of variation in the trait (and usually with %RMSE < 10%; complete results are in the Supplement).

Mapping and application

We used the PLSR-derived coefficients (Supplement) to generate spatially explicit maps of traits and respective uncertainties. We show a subset from one of the many scenes used in this study (Green Ridge State Forest, Maryland, USA; Fig. 7).With these maps, we synthesized spatial patterns in foliar traits into images of functional variation using false color composites of key foliar traits such as nitrogen, lignin, and leaf mass per area (Appendix: Fig. A6). Such maps illustrate gradients of canopy biochemical and morphological traits that are likely to be related to species associations and provide greater detail than traditional land cover maps. The trait maps expose patterns of plant investment in foliar nutrients vs. structural compounds across environmental gradients on the landscape. Comparison of trait maps among regions reveals variability in relative abundance of traits inferred from, but not captured by, land cover classifications (Appendix: Fig. A6). Maps of functional traits from a single hyperspectral image can reveal differences in species associations across gradients that are otherwise only apparent in multi-date imagery (Appendix: Fig. A7), and, moreover, can help to identify ecosystem-level consequences of disturbance events through changes in functional traits and mapped uncertainty (Appendix: Fig. A8).

DISCUSSION

In this study we confirm the capacity of imaging spectroscopy to accurately and repeatedly map foliar traits important for describing landscape patterns in nutrient cycling (e.g., Chapin 2003, Kazakou et al. 2006, Quested et al. 2007, Santiago 2007) and photosynthetic capacity (e.g., Kattge et al. 2009).The approach was robust across multiple traits, using data from numerous sites, vegetation types, and years. Our method for estimating canopy chemistry integrated three scales of observation—leaf spectra, plot structure, and image spectra—thus allowing the propagation of uncertainty from the leaf-level dependent variables to the plot and canopy levels, and finally to maps created from image spectra. Although imaging spectroscopy has been used in several studies to map foliar traits (Wessman et al.
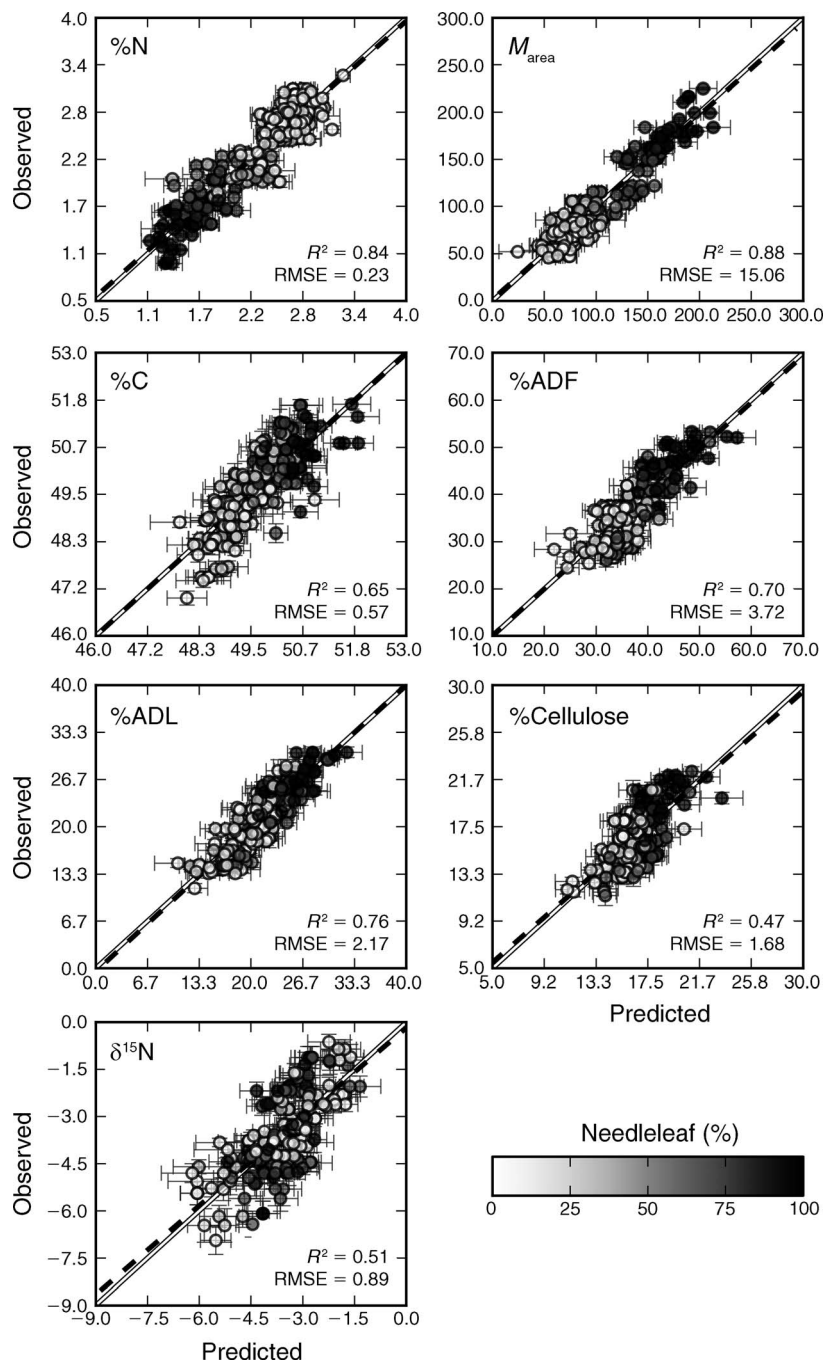
FIG. 4. PLSR model fits using AVIRIS-derived spectra fitted to foliar traits scaled from leaves to the canopy. Model performance was evaluated by averaging 500 randomized models built with a 50/50 calibration/validation split. Horizontal bars indicate uncertainty (1 SD) in predictions; vertical bars indicate uncertainty (1 SD) in plot-level estimates propagated from leaf-level measurements. The shading scheme of dots indicates increasing relative biomass of needleleaf foliage (white to black). Abbreviations are: M_{area}, leaf mass per area; %ADF, acid detergent fiber; %ADL, acid detergent lignin; RMSE, root mean square error.

1989, Curran et al. 1997, Serrano et al. 2002, Townsend et al. 2003, Huber et al. 2008, Martin et al. 2008), ours demonstrates the capacity to map multiple functional traits across a diversity of sites, years, images, and geographic complexity, as well as to explicitly account for the propagation of measurement, scaling, and modeling uncertainty through to the end product.

The per trait waveband calibration coefficients provide a basis for physiological interpretation of the results as well as the assessment of the results' generality
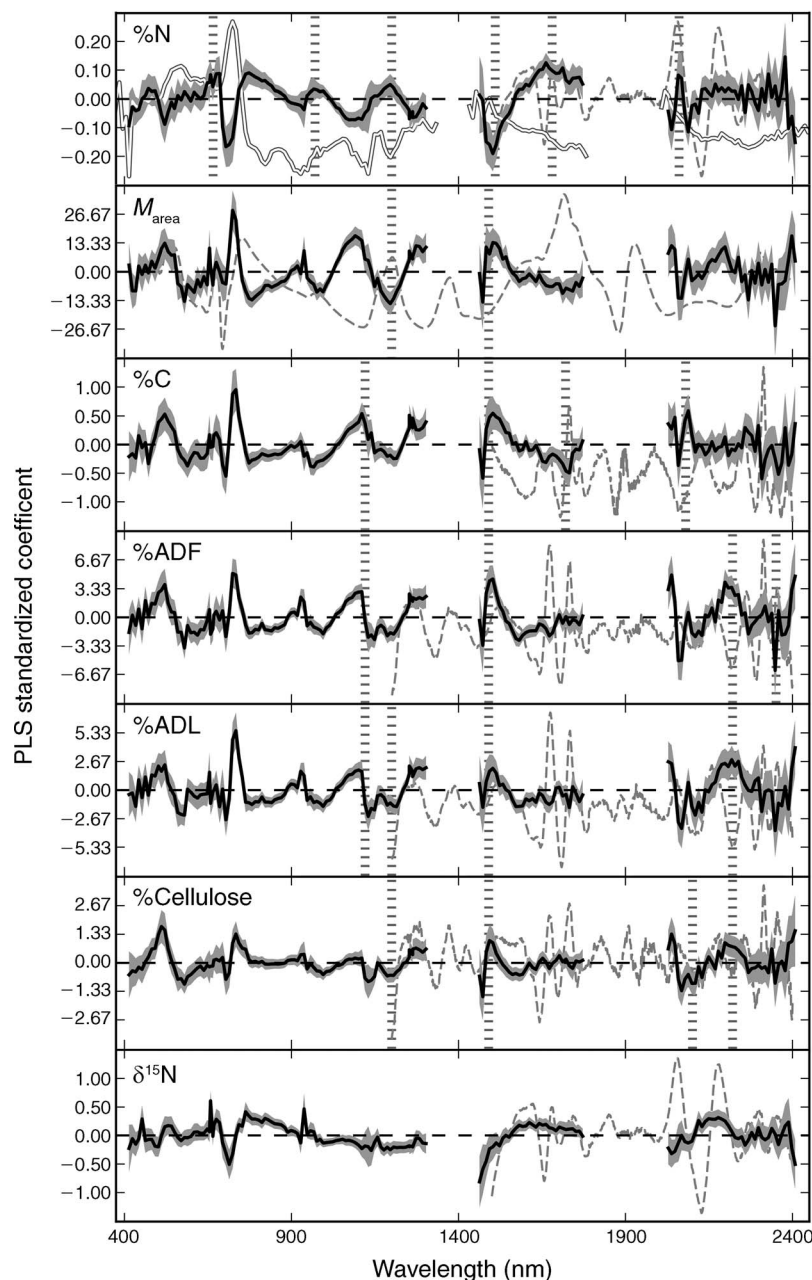
Fig. 5. Standardized PLSR coefficients indicating the magnitude and direction of influence of each wavelength (with ± 1 SD bands in gray). Note that raw coefficients are applied to image spectra to derive spatial predictions. Short vertical gray bars are absorption features at wavelengths known from previous studies. Dashed gray curves indicate standardized coefficients from Serbin et al. (2014); the white-filled line in the %N panel represents coefficients from Martin et al. (2008).

for mapping to other data sets. The important wavebands align with fresh-leaf results for M_{area} and dry-sample results for chemical constituents reported by Serbin et al. (2012, 2014), as well as with wavebands indicated by Martin et al. (2008) as important for foliar nitrogen from AVIRIS (Fig. 5). In comparison with leaf-level results, standardized coefficients matched across most of the spectrum, but there was a reversal of sign in coefficients across the red edge (500–700 nm).

Leaf-level NIR reflectance results from scattering at the interface between cell walls and intercellular air spaces, whereas canopy (i.e., image) reflectance is strongly dominated by canopy structural properties such as leaf clumping, angle, and density (Jacquemoud et al. 2009, Sullivan et al. 2013). For instance, leaf-level NIR reflectance generally increases with thickness of needle leaves (Ehleringer and Mooney 1978, Lin and Ehleringer 1983, DeLucia et al. 1996, Slaton et al. 2001), but
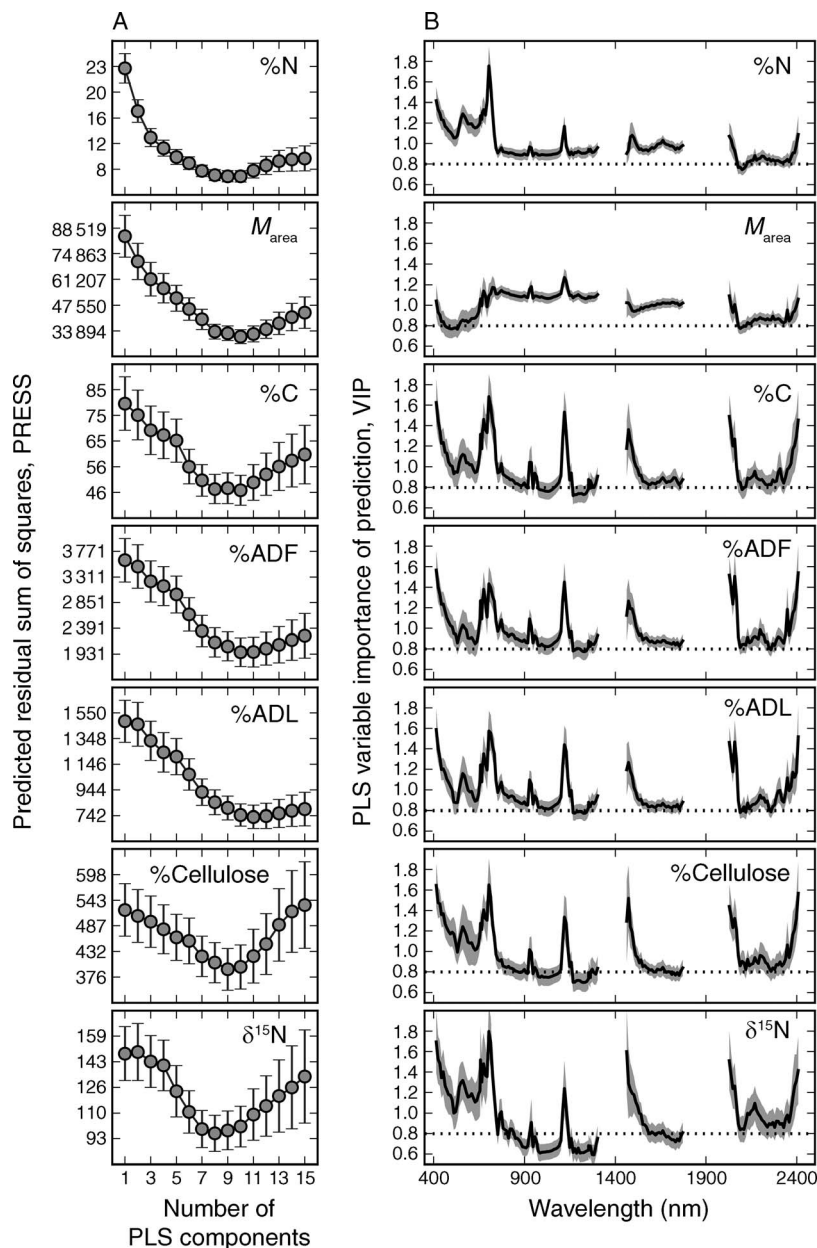
FIG. 6. (A) Profile of the PRESS (predicted residual sum of squares) statistic (with ± 1 SD bars) obtained by fitting 500 randomized models, each using an increasing number of PLS components (h, on the x-axis). The final model was fit using the components that minimized the PRESS statistic. (B) Profile of the VIP (variable importance of prediction) statistic with ± 1 SD gray bands. The VIP describes the relative importance of each wavelength in predicting the quantity of interest, and is considered significant where VIP > 0.8 (dotted line).

canopy-level NIR reflectance decreases with greater abundance of needleleaf species because absorption-inducing canopy properties (e.g., greater needle clumping) overwhelm leaf traits in affecting NIR canopy reflectance (Ollinger 2011, Sullivan et al. 2013). Considering recent critiques of imaging spectroscopy-based trait mapping (Knyazikhin et al. 2013), this switch in the direction of NIR coefficients between leaf and canopy-level models of M_{area} provides added confidence that

imaging spectroscopy captures sufficient information about the canopy and constituent foliage for purposes of mapping (Ollinger et al. 2013, Townsend et al. 2013). Moreover, the striking similarity of results obtained from the four schemes to scale canopy-height-related differences in measured leaf traits (Appendix A) further supports recent work emphasizing the mass basis for measuring variability in the global leaf economics spectrum (Niinemets et al. 2014), and again underscores

TABLE 3. Summary of PLSR (partial least squares regression) models built using AVIRIS spectra and foliar traits scaled to the plot level.

Trait	Traits		Model			Calibration		Validation		Model-averaged	
	Mean (SD)	Range	N	Train%	h	R^2	RMSE	R^2	RMSE	R^2	RMSE
M_{area}	107.28 (43.09)	51.88–224.53	202	28.82	10	0.92 (0.016)	12.68 (1.177)	0.81 (0.027)	18.20 (1.273)	0.88	15.039
%N	2.21 (0.56)	0.96–3.31	212	29.94	10	0.90 (0.019)	0.19 (0.016)	0.77 (0.028)	0.26 (0.015)	0.85	0.218
%C	49.68 (0.93)	46.94–51.73	208	29.47	10	0.67 (0.054)	0.55 (0.049)	0.44 (0.068)	0.69 (0.049)	0.63	0.568
%ADF	36.78 (7.10)	23.15–53.01	214	30.07	10	0.77 (0.041)	3.56 (0.317)	0.49 (0.062)	4.89 (0.299)	0.68	4.005
%ADL	20.99 (4.66)	10.53–30.57	211	29.50	12	0.86 (0.033)	1.80 (0.198)	0.52 (0.064)	3.16 (0.209)	0.74	2.343
%Cellulose	16.39 (2.50)	10.26–22.54	213	29.67	9	0.63 (0.059)	1.66 (0.151)	0.27 (0.062)	2.10 (0.104)	0.49	1.781
$\delta^{15}N$	−3.53 (1.33)	−6.90 to −0.74	190	28.30	8	0.59 (0.066)	0.89 (0.087)	0.29 (0.059)	1.14 (0.062)	0.48	0.954

Notes: Means of coefficients of determination (R^2) and associated root mean squared error (RMSE) statistics of 500 randomized models are presented along with associated uncertainty estimates (SD). Model-averaged fits indicate the accuracies obtained at the image level after averaging predictions from 500 models. Train% is the fraction of data used for model calibration; h is the number of components used to build PLSR models.

the robust ability of imaging spectroscopy to map spatial patterns from canopy-scale measurements.

We compared coefficients obtained from our analysis of %N with those published by Martin et al. (2008), the only other study using comparable multi-scene and multi-location data. Loadings of standardized coefficients for our models generally agreed with the Martin et al. models (2008); see Fig. 5. Discrepancies in locations of dips and spikes in coefficients result primarily from our use of a standardized data set (i.e., centered and scaled) compared to raw coefficients from Martin et al. (2008). Martin et al. (2008) employed 11 images (5 AVIRIS, 6 Hyperion) covering a wide variety of temperate and tropical forest ecosystems in North America and Australia; theirs was the first study to show the potential for building general models to map foliar traits across large regions.

While not as global in scope as Martin et al. (2008), our analysis incorporates multiple forest types dominated by a range of broadleaf and conifer species (Appendix: Table A2; Supplement; see Serbin et al. 2014), and covers the breadth of forest functional variability within North American eastern temperate forests. Any missing species and forest types probably are bracketed by the range of our data, and we expect that spatial patterns of uncertainties (e.g., Fig. 7) are indicative of gaps in our database for different forest optical types (sensu Ustin and Gamon 2010) rather than weaknesses in model performance. The largest uncertainties were observed in locations where (1) the vegetation was not represented in our database of foliar traits due to our focus on forests (i.e., grasses, forbs, crops, wetlands); (2) there were strong terrain effects in the imagery not fully accounted for in the topographic normalization; or (3) along forest edges and disturbed areas. In particular, the uncertainty mapping helped to identify areas that had been recently disturbed (Appen-

dix: Fig A8). Logged areas showed a consistent pattern of higher lignin and M_{area} and lower foliar nitrogen content (and also higher $\delta^{15}N$, indicating increased N availability) compared to adjacent undisturbed areas. Although such patterns are not unexpected, those areas also had consistently high uncertainties due to optical properties of disturbances being on the edge of the range of variability of optical properties for the intact forests we sampled. Future analysis of vegetation traits in disturbed areas using imaging spectroscopy may provide the opportunity to better understand changes in ecosystem dynamics brought about by human or natural perturbations.

Composite maps of functional traits (e.g., Appendix: Fig A6) revealed a greater amount of variability in forest canopies than apparent in individual maps, and in particular, land cover classifications. For example, in the Central Appalachian sites, codominant conifers in ridges and valleys were revealed by the higher lignin content and M_{area} of conifers (Fig.7). Comparisons between maps of individual traits (Fig. 7) also revealed gradients in functional traits that follow the inverse relationship between investments in leaf structural mass in contrast to leaf nutrients (Wright and Westoby 2002, Reich et al. 2003, Wright et al. 2004). Regions showing higher foliar nitrogen concentrations were associated with lower values of M_{area} and vice versa. Although this is widely known from multiple species inhabiting diverse ecosystems (Reich et al. 1998, 1999, Wright et al. 2001, Sanchez-Azofeifa et al. 2009, Asner et al. 2011b), imaging spectroscopy allowed these associations to be mapped explicitly and across multiple ecoregions.

The geographic patterns in trait variability matched expectations associated with climate and other environmental drivers (Table 2). For example, the negative correlation between M_{area} and leaf nitrogen is in agreement with the broader concept of the leaf economic
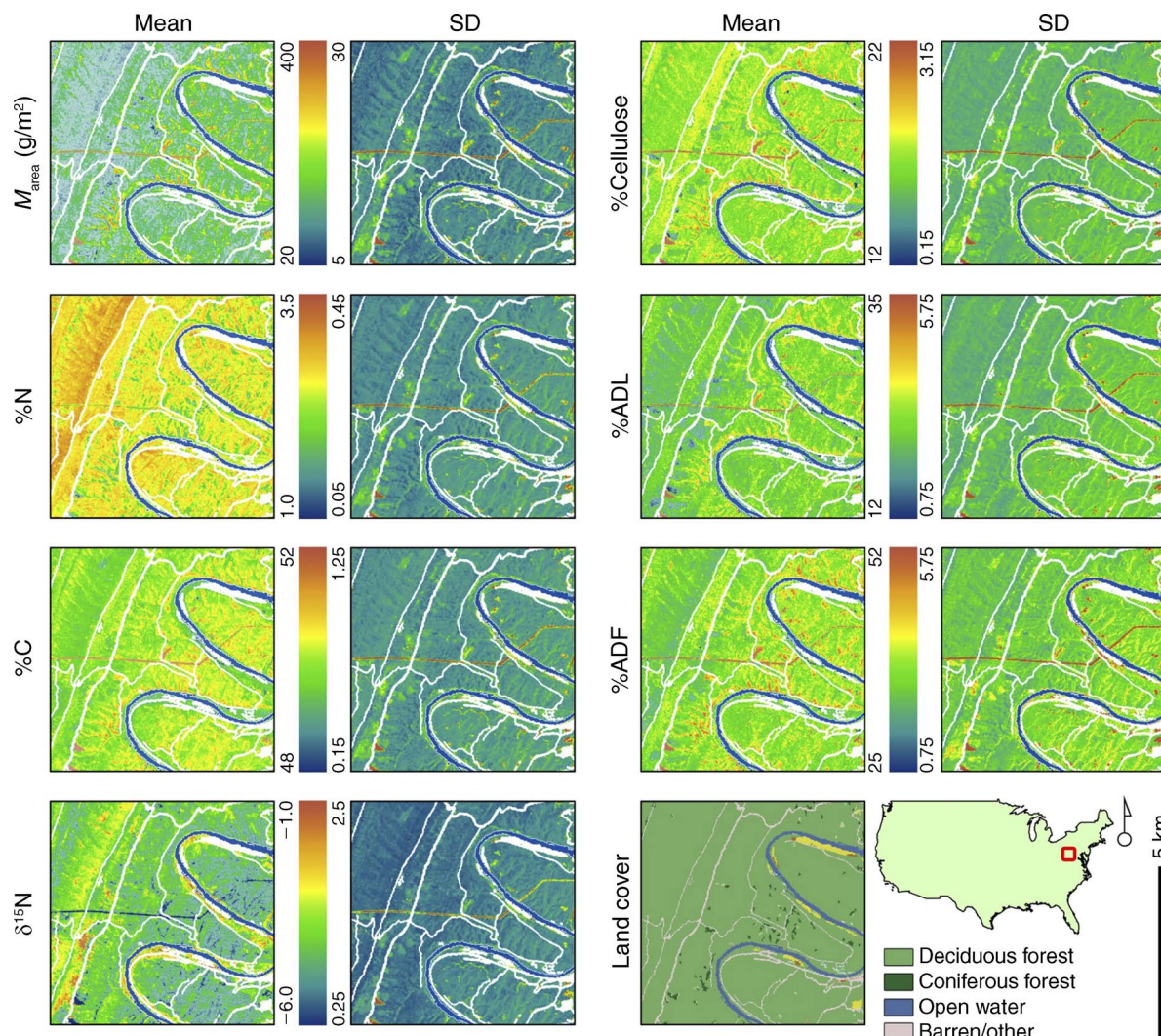
Fig. 7. Spatial predictions of M_{area}, %N, %C, δ^{15}N, %Cellulose, %ADL, and %ADF means (left panels) and uncertainties, i.e., standard deviations (right panels), obtained by applying 500 sets of coefficients obtained from randomized PLSR models to AVIRIS imagery acquired over the Green Ridge State Forest, Maryland (Fig. 1, box F). Each model was built with a 50/50 calibration/validation split. See Table 3 for model statistics and the Supplement for raw PLSR coefficients.

spectrum (Wright et al. 2004, 2005*a*, *b*). The positive correlation of foliar N with regional-scale N deposition corroborates evidence of foliar N enrichment reported in numerous studies in northeastern forests (McNeil et al. 2007, 2012, Davis et al. 2009, Crowley et al. 2012). Correlations of foliar δ^{15}N concentrations with mean annual temperature (positive) and precipitation (negative) agree with results in Amundson et al. (2003), Craine et al. (2009), and Serbin et al. (2014). Mapped evidence of increased isotopic N along the N deposition gradient corroborates Emmett et al. (1998) and Mc-Lauchlan et al. (2007), showing that greater N availability yields less preferential retention of lighter ^{14}N in the soil system.

It has been recently demonstrated that estimates of canopy structure and composition obtained from imaging spectroscopy are invaluable in constraining regional carbon flux models (Antonarakis et al. 2014). Maps of foliar traits obtained from this study can be leveraged to drive ecosystem process models requiring parameterization of foliar nitrogen content and leaf mass per area, which are coordinated in leaves to maximize carbon fixation (Shipley et al. 2005) in patterns independent of species-level physiognomy (Reich et al. 1991, 1992, Grime 2006).This offers the potential to develop data sets needed to drive spatially explicit ecosystem process models at large scales from proposed forthcoming satellites(e.g., HyspIRI, EnMAP: see Stuffler et al. 2007, Middleton et al. 2013). Although spatial patterns of canopy foliar N, lignin, and M_{area} are largely interpretable in terms of species associations, patterns of δ^{15}N will require considerable follow-up field

research. In locations where $\delta^{15}N$ concentrations appear elevated without associated increased uncertainties or changes in foliar N and or M_{area} (indicating an obvious change in plant functional associations), localized patterns of $\delta^{15}N$ enrichment (for e.g., see Fig. 7, SE corner in $\delta^{15}N$ map) could be an indicator of elevated N availability via ephemeral disturbances such as insect defoliation or logging. The availability of spatial predictions of foliar traits may therefore open up new investigations into biotic or abiotic nutrient cycling controls across both small regions and large landscapes.

Imaging spectroscopy offers the opportunity for applications ranging from assessment of biochemical effects of invasive species (Glenn et al. 2005, Asner et al. 2008, He et al. 2011), to characterizing photosynthetic down-regulation (Gamon et al. 1990, 1992, 1997) and measurement of the inductance of plant defense to perturbations (Couture et al. 2013). By directly measuring the chemical and physiological consequences of disturbances and other environmental drivers on vegetation, space-borne imaging spectroscopy should provide the ability to directly quantify the consequences of environmental change rather than inferring it from land cover maps or vegetation indices. This will provide agencies the tools to measure impacts of invasions or help to better guide management activities.

Conclusions

Using data from a wide range of forest ecosystems, we rigorously tested the capacity of imaging spectroscopy to map multiple forest functional traits. The resulting maps enable us to describe fundamental axes of variability in plant physiology along a spectrum ranging from "fast" (high nutrients and low lignin, thin, low M_{area} leaves) to "slow" patterns of forest nutrient cycling (Reich et al. 1991, 1992, 1999, Craine et al. 2002, Wright et al. 2005a, b, Sanchez-Azofeifa et al. 2009). It is exciting to begin answering questions on the spatial patterns in these traits, but ultimately, trait mapping from imaging spectroscopy is likely to have its greatest impact by enabling researchers to pose more applied questions. For example: how does functional biogeography (Violle et al. 2014) mediate ecosystem response to environmental change? By helping to answer such questions, multiple-trait mapping, coupled with robust assessments of its uncertainty, opens up the potential for making defensible, tractable, and scalable predictions of the delivery of key ecosystem services from complex forest environments that are increasingly subjected to multiple agents of global environmental change.

Our work accomplishes two objectives: we provide a set of equations (Supplement) that can be used with imaging spectroscopy data to maps traits in similar environments (temperate forests). As well, we outline a workflow that could be implemented in other ecosystem types. An important next step for trait mapping is the integration of data collected from across the globe

(Asner and Martin 2009, Asner et al. 2012). This integration will further determine the extent of the generality of these methods, with respect to sensor types, measurement or analytical strategies, and environmental variability. Coupled with other studies, this research represents a step toward the development of global approaches to mapping plant functional properties from imaging spectroscopy, and thus helps to provide a more solid foundation for the development of "trait" products from the proposed HyspIRI mission and NEON's Aerial Observatory Platform (Kampe et al. 2010, Middleton et al. 2013, Sims et al. 2013).

Literature Cited

Ainsworth, E. A., and A. Rogers. 2007. The response of photosynthesis and stomatal conductance to rising CO_2: mechanisms and environmental interactions. Plant Cell and Environment 30:258–270.

Altman, D. G., and P. K. Andersen. 1989. Bootstrap investigation of the stability of a Cox regression-model. Statistics in Medicine 8:771–783.

Amundson, R., A. T. Austin, E. A. G. Schuur, K. Yoo, V. Matzek, C. Kendall, A. Uebersax, D. Brenner, and W. T. Baisden. 2003. Global patterns of the isotopic composition of soil and plant nitrogen. Global Biogeochemical Cycles 17(1):1031.

Antonarakis, A. S., J. W. Munger, and P. R. Moorcroft. 2014. Imaging spectroscopy- and lidar-derived estimates of canopy composition and structure to improve predictions of forest carbon fluxes and ecosystem dynamics. Geophysical Research Letters 41:2535–2542.

Asner, G. P. 1998. Biophysical and biochemical sources of variability in canopy reflectance. Remote Sensing of Environment 64:234–253.

Asner, G. P., M. O. Jones, R. E. Martin, D. E. Knapp, and R. F. Hughes. 2008. Remote sensing of native and invasive species in Hawaiian forests. Remote Sensing of Environment 112:1912–1926.

Asner, G. P., D. E. Knapp, J. Boardman, R. O. Green, T. Kennedy-Bowdoin, M. Eastwood, R. E. Martin, C. Anderson, and C. B. Field. 2012. Carnegie Airborne Observatory-2: Increasing science data dimensionality via high-fidelity multi-sensor fusion. Remote Sensing of Environment 124:454–465.

Asner, G. P., and R. E. Martin. 2008. Spectral and chemical analysis of tropical forests: scaling from leaf to canopy levels. Remote Sensing of Environment 112:3958–3970.

Asner, G. P., and R. E. Martin. 2009. Airborne spectranomics: mapping canopy chemical and taxonomic diversity in tropical forests. Frontiers in Ecology and the Environment 7:269–276.

Asner, G. P., R. E. Martin, D. E. Knapp, R. Tupayachi, C. Anderson, L. Carranza, P. Martinez, M. Houcheime, F. Sinca, and P. Weiss. 2011a. Spectroscopy of canopy chemicals in humid tropical forests. Remote Sensing of Environment 115:3587–3598.

Asner, G. P., R. E. Martin, R. Tupayachi, R. Emerson, P. Martinez, F. Sinca, G. V. N. Powell, S. J. Wright, and A. E. Lugo. 2011b. Taxonomy and remote sensing of leaf mass per area (LMA) in humid tropical forests. Ecological Applications 21:85–98.

Asner, G. P., and P. M. Vitousek. 2005. Remote analysis of biological invasion and biogeochemical change. Proceedings of the National Academy of Sciences USA 102:4383–4386.

Austin, A. T., and P. M. Vitousek. 1998. Nutrient dynamics on a precipitation gradient in Hawai'i. Oecologia 113:519–529.

Baret, F., V. C. Vanderbilt, M. D. Steven, and S. Jacquemoud. 1994. Use of spectral analogy to evaluate canopy reflectance sensitivity to leaf optical-properties. Remote Sensing of Environment 48:253–260.

Berg, B. 2000. Litter decomposition and organic matter turnover in northern forest soils. Forest Ecology and Management 133:13–22.

Blackburn, G. A. 2007. Hyperspectral remote sensing of plant pigments. Journal of Experimental Botany 58:855–867.

Bonan, G. B. 1993. Physiological controls of the carbon balance of boreal forest ecosystems. Canadian Journal of Forest Research 23:1453–1471.

Carrera, A. L., and M. B. Bertiller. 2010. Relationships among plant litter, fine roots, and soil organic C and N across an aridity gradient in northern Patagonia, Argentina. Ecoscience 17:276–286.

Chapin, F. S. 2003. Effects of plant traits on ecosystem and regional processes: a conceptual framework for predicting the consequences of global change. Annals of Botany 91:455–463.

Chapin, F. S., M. S. BretHarte, S. E. Hobbie, and H. L. Zhong. 1996. Plant functional types as predictors of transient responses of arctic vegetation to global change. Journal of Vegetation Science 7:347–358.

Chen, S., X. Hong, C. J. Harris, and P. M. Sharkey. 2004. Sparse modeling using orthogonal forward regression with PRESS statistic and regularization. IEEE Transactions on Systems, Man and Cybernetics B 34:898–911.

Collatz, G. J., M. Ribas-Carbo, and J. A. Berry. 1992. Coupled photosynthesis–stomatal conductance model for leaves of C4 plants. Australian Journal of Plant Physiology 19:519–538.

Coops, N. C., M. L. Smith, M. E. Martin, and S. V. Ollinger. 2003. Prediction of eucalypt foliage nitrogen content from satellite-derived hyperspectral data. IEEE Transactions on Geoscience and Remote Sensing 41:1338–1346.

Couture, J. J., S. P. Serbin, and P. A. Townsend. 2013. Spectroscopic sensitivity of real-time, rapidly induced phytochemical change in response to damage. New Phytologist 198:311–319.

Craine, J. M., et al. 2009. Global patterns of foliar nitrogen isotopes and their relationships with climate, mycorrhizal fungi, foliar nutrient concentrations, and nitrogen availability. New Phytologist 183:980–992.

Craine, J. M., D. Tilman, D. Wedin, P. Reich, M. Tjoelker, and J. Knops. 2002. Functional traits, productivity and effects on nitrogen cycling of 33 grassland species. Functional Ecology 16:563–574.

Cramer, W., et al. 2001. Global response of terrestrial ecosystem structure and function to CO_2 and climate change: results from six dynamic global vegetation models. Global Change Biology 7:357–373.

Crowley, K. F., et al. 2012. Do nutrient limitation patterns shift from nitrogen toward phosphorus with increasing nitrogen deposition across the northeastern United States? Ecosystems 15:940–957.

Curran, P. J. 1989. Remote-sensing of foliar chemistry. Remote Sensing of Environment 30:271–278.

Curran, P. J., J. L. Dungan, B. A. Macler, S. E. Plummer, and D. L. Peterson. 1992. Reflectance spectroscopy of fresh whole leaves for the estimation of chemical concentration. Remote Sensing of Environment 39:153–166.

Curran, P. J., J. L. Dungan, and D. L. Peterson. 2001. Estimating the foliar biochemical concentration of leaves with reflectance spectrometry testing the Kokaly and Clark methodologies. Remote Sensing of Environment 76:349–359.

Curran, P. J., J. A. Kupiec, and G. M. Smith. 1997. Remote sensing the biochemical composition of a slash pine canopy. IEEE Transactions on Geoscience and Remote Sensing 35:415–420.

Davis, S. C., K. E. Dragan, C. R. Buyarski, and R. B. Thomas. 2009. High foliar and soil nitrogen concentrations in central Appalachian forests. Ecosystems 12:46–56.

Deel, L. N., B. E. McNeil, P. G. Curtis, S. P. Serbin, A. Singh, K. N. Eshleman, and P. A. Townsend. 2012. Relationship of a Landsat cumulative disturbance index to canopy nitrogen and forest structure. Remote Sensing of Environment 118:40–49.

DeLucia, E. H., K. Nelson, T. C. Vogelmann, and W. K. Smith. 1996. Contribution of intercellular reflectance to photosynthesis in shade leaves. Plant Cell and Environment 19:159–170.

Diaz, S., et al. 2004. The plant traits that drive ecosystems: evidence from three continents. Journal of Vegetation Science 15:295–304.

Ehleringer, J. R., and H. A. Mooney. 1978. Leaf hairs: effects on physiological activity and adaptive value to a desert shrub. Oecologia 37:183–200.

Emmett, B. A., O. J. Kjonaas, P. Gundersen, C. Koopmans, A. Tietema, and D. Sleep. 1998. Natural abundance of N^{15} in forests across a nitrogen deposition gradient. Forest Ecology and Management 101:9–18.

Enquist, B. J., A. J. Kerkhoff, T. E. Huxman, and E. P. Economo. 2007. Adaptive differences in plant physiology and ecosystem paradoxes: insights from metabolic scaling theory. Global Change Biology 13:591–609.

Fortunel, C., et al. 2009. Leaf traits capture the effects of land use changes and climate on litter decomposability of grasslands across Europe. Ecology 90:598–611.

Fourty, T., F. Baret, S. Jacquemoud, G. Schmuck, and J. Verdebout. 1996. Leaf optical properties with explicit description of its biochemical composition: direct and inverse problems. Remote Sensing of Environment 56:104–117.

Frank, I. E., and J. H. Friedman. 1993. A statistical view of some chemometrics regression tools. Technometrics 35:109–135.

Friedlingstein, P., et al. 2014. Persistent growth of CO_2 emissions and implications for reaching climate targets. Nature Geoscience 7:709–715.

Gamon, J. A., C. B. Field, W. Bilger, O. Bjorkman, A. L. Fredeen, and J. Penuelas. 1990. Remote-sensing of the xanthophyll cycle and chlorophyll fluorescence in sunflower leaves and canopies. Oecologia 85:1–7.

Gamon, J. A., J. Penuelas, and C. B. Field. 1992. A narrow-waveband spectral index that tracks diurnal changes in photosynthetic efficiency. Remote Sensing of Environment 41:35–44.

Gamon, J. A., L. Serrano, and J. S. Surfus. 1997. The photochemical reflectance index: an optical indicator of photosynthetic radiation use efficiency across species, functional types, and nutrient levels. Oecologia 112:492–501.

Gao, B. C., M. J. Montes, Z. Ahmad, and C. O. Davis. 2000. Atmospheric correction algorithm for hyperspectral remote sensing of ocean color from space. Applied Optics 39:887–896.

Gates, D. M., H. J. Keegan, J. C. Schleter, and V. R. Weidner. 1965. Spectral properties of plants. Applied Optics 4:11–20.

Geladi, P., and B. R. Kowalski. 1986. Partial least-squares regression: a tutorial. Analytica Chimica Acta 185:1–17.

Glenn, N. F., J. T. Mundt, K. T. Weber, T. S. Prather, L. W. Lass, and J. Pettingill. 2005. Hyperspectral data processing for repeat detection of small infestations of leafy spurge. Remote Sensing of Environment 95:399–412.

Green, D. S., J. E. Erickson, and E. L. Kruger. 2003. Foliar morphology and canopy nitrogen as predictors of light-use efficiency in terrestrial vegetation. Agricultural and Forest Meteorology 115:163–171.

Green, R. O., et al. 1998. Imaging spectroscopy and the Airborne Visible Infrared Imaging Spectrometer (AVIRIS). Remote Sensing of Environment 65:227–248.

Grime, J. P. 2006. Trait convergence and trait divergence in herbaceous plant communities: mechanisms and consequences. Journal of Vegetation Science 17:255–260.

Grossman, Y. L., S. L. Ustin, S. Jacquemoud, E. W. Sanderson, G. Schmuck, and J. Verdebout. 1996. Critique of stepwise multiple linear regression for the extraction of leaf biochemistry information from leaf reflectance data. Remote Sensing of Environment 56:182–193.

Hattenschwiler, S., A. V. Tiunov, and S. Scheu. 2005. Biodiversity and litter decomposition in terrestrial ecosystems. Annual Review of Ecology, Evolution, and Systematics 36:191–218.

He, K. S., D. Rocchini, M. Neteler, and H. Nagendra. 2011. Benefits of hyperspectral remote sensing for tracking plant invasions. Diversity and Distributions 17:381–392.

Hobbie, E. A., S. A. Macko, and M. Williams. 2000. Correlations between foliar δN^{15} and nitrogen concentrations may indicate plant–mycorrhizal interactions. Oecologia 122:273–283.

Hobbie, S. E., M. Ogdahl, J. Chorover, O. A. Chadwick, J. Oleksyn, R. Zytkowiak, and P. B. Reich. 2007. Tree species effects on soil organic matter dynamics: the role of soil cation composition. Ecosystems 10:999–1018.

Hogberg, P. 1997. Tansley review No 95. N^{15} natural abundance in soil–plant systems. New Phytologist 137:179–203.

Huber, S., M. Kneubuhler, A. Psomas, K. Itten, and N. E. Zimmermann. 2008. Estimating foliar biochemistry from hyperspectral data in mixed forest canopy. Forest Ecology and Management 256:491–501.

Jacquemoud, S., W. Verhoef, F. Baret, C. Bacour, P. J. Zarco-Tejada, G. P. Asner, C. Francois, and S. L. Ustin. 2009. PROSPECT plus SAIL models: A review of use for vegetation characterization. Remote Sensing of Environment 113:S56–S66.

Jenkins, J. C., D. C. Chojnacky, L. S. Heath, and R. A. Birdsey. 2003. National-scale biomass estimators for United States tree species. Forest Science 49:12–35.

Johnson, J. M. F., N. W. Barbour, and S. L. Weyers. 2007. Chemical composition of crop biomass impacts its decomposition. Soil Science Society of America Journal 71:155–162.

Kampe, T. U., B. R. Johnson, M. Kuester, and M. Keller. 2010. NEON: the first continental-scale ecological observatory with airborne remote sensing of vegetation canopy biochemistry and structure. Journal of Applied Remote Sensing 4:043510.

Kattge, J., W. Knorr, T. Raddatz, and C. Wirth. 2009. Quantifying photosynthetic capacity and its relationship to leaf nitrogen content for global-scale terrestrial biosphere models. Global Change Biology 15:976–991.

Kazakou, E., D. Vile, B. Shipley, C. Gallet, and E. Garnier. 2006. Co-variations in litter decomposition, leaf traits and plant growth in species from a Mediterranean old-field succession. Functional Ecology 20:21–30.

Kazakou, E., C. Violle, C. Roumet, C. Pintor, O. Gimenez, and E. Garnier. 2009. Litter quality and decomposability of species from a Mediterranean succession depend on leaf traits but not on nitrogen supply. Annals of Botany 104:1151–1161.

Kergoat, L., S. Lafont, A. Arneth, V. Le Dantec, and B. Saugier. 2008. Nitrogen controls plant canopy light-use efficiency in temperate and boreal ecosystems. Journal of Geophysical Research-Biogeosciences 113:G04017.

Knorr, M., S. D. Frey, and P. S. Curtis. 2005. Nitrogen additions and litter decomposition: a meta-analysis. Ecology 86:3252–3257.

Knyazikhin, Y., et al. 2013. Hyperspectral remote sensing of foliar nitrogen content. Proceedings of the National Academy of Sciences USA 110:E185–E192.

Kokaly, R. F. 2001. Investigating a physical basis for spectroscopic estimates of leaf nitrogen concentration. Remote Sensing of Environment 75:153–161.

Kokaly, R. F., G. P. Asner, S. V. Ollinger, M. E. Martin, and C. A. Wessman. 2009. Characterizing canopy biochemistry from imaging spectroscopy and its application to ecosystem studies. Remote Sensing of Environment 113:S78–S91.

Le Quere, C., et al. 2009. Trends in the sources and sinks of carbon dioxide. Nature Geoscience 2:831–836.

Lilleskov, E. A., E. A. Hobbie, and T. J. Fahey. 2002. Ectomycorrhizal fungal taxa differing in response to nitrogen deposition also differ in pure culture organic nitrogen use and natural abundance of nitrogen isotopes. New Phytologist 154:219–231.

Lin, Z. F., and J. Ehleringer. 1983. Epidermis effects on spectral properties of leaves of four herbaceous species. Physiologia Plantarum 59:91–94.

Long, S. P. 1991. Modification of the response of photosynthetic productivity to rising temperature by atmospheric CO_2 concentrations: Has its importance been underestimated? Plant Cell and Environment 14:729–739.

Lucht, W., C. B. Schaaf, and A. H. Strahler. 2000. An algorithm for the retrieval of albedo from space using semiempirical BRDF models. IEEE Transactions on Geoscience and Remote Sensing 38:977–998.

Martin, M. E., and J. D. Aber. 1997. High spectral resolution remote sensing of forest canopy lignin, nitrogen, and ecosystem processes. Ecological Applications 7:431–443.

Martin, M. E., L. C. Plourde, S. V. Ollinger, M. L. Smith, and B. E. McNeil. 2008. A generalizable method for remote sensing of canopy nitrogen across a wide range of forest ecosystems. Remote Sensing of Environment 112:3511–3519.

Martinelli, L. A., M. C. Piccolo, A. R. Townsend, P. M. Vitousek, E. Cuevas, W. McDowell, G. P. Robertson, O. C. Santos, and K. Treseder. 1999. Nitrogen stable isotopic composition of leaves and soil: tropical versus temperate forests. Biogeochemistry 46:45–65.

Matson, P., L. Johnson, C. Billow, J. Miller, and R. L. Pu. 1994. Seasonal patterns and remote spectral estimation of canopy chemistry across the Oregon transect. Ecological Applications 4:280–298.

McClaugherty, C., and B. Berg. 1987. Cellulose, lignin and nitrogen concentrations as rate regulating factors in late stages of forest litter decomposition. Pedobiologia 30:101–112.

McLauchlan, K. K., J. M. Craine, W. W. Oswald, P. R. Leavitt, and G. E. Likens. 2007. Changes in nitrogen cycling during the past century in a northern hardwood forest. Proceedings of the National Academy of Sciences USA 104:7466–7470.

McNeil, B. E., K. M. de Beurs, K. N. Eshleman, J. R. Foster, and P. A. Townsend. 2007. Maintenance of ecosystem nitrogen limitation by ephemeral forest disturbance: An assessment using MODIS, Hyperion, and Landsat ETM. Geophysical Research Letters 34:L19406.

McNeil, B. E., J. M. Read, and C. T. Driscoll. 2012. Foliar nitrogen responses to the environmental gradient matrix of the Adirondack Park, New York. Annals of the Association of American Geographers 102:1–16.

McNeil, B. E., J. M. Read, T. J. Sullivan, T. C. McDonnell, I. J. Fernandez, and C. T. Driscoll. 2008. The spatial pattern of nitrogen cycling in the Adirondack Park, New York. Ecological Applications 18:438–452.

Meier, C. L., and W. D. Bowman. 2008. Links between plant litter chemistry, species diversity, and below-ground ecosys-

tem function. Proceedings of the National Academy of Sciences USA 105:19780–19785.

Melillo, J. M., J. D. Aber, and J. F. Muratore. 1982. Nitrogen and lignin control of hardwood leaf litter decomposition dynamics. Ecology 63:621–626.

Menesatti, P., F. Antonucci, F. Pallottino, G. Roccuzzo, M. Allegra, F. Stagno, and F. Intrigliolo. 2010. Estimation of plant nutritional status by Vis-NIR spectrophotometric analysis on orange leaves *Citrus sinensis* (L) Osbeck cv Tarocco. Biosystems Engineering 105:448–454.

Middleton, E. M., S. G. Ungar, D. J. Mandl, L. Ong, S. W. Frye, P. E. Campbell, D. R. Landis, J. P. Young, and N. H. Pollack. 2013. The Earth Observing One (EO-1) Satellite mission: over a decade in space. IEEE Journal of Selected Topics in Applied Earth Observations and Remote Sensing 6:243–256.

Montes, M. J., and B.-C. Gao. 2004. NRL atmospheric correction algorithms for oceans: TAFKAA users' guide. Naval Research Laboratory, Washington, D.C., USA.

NADP. 2014. National Atmospheric Deposition Program. NADP Program Office, Illinois State Water Survey, Champaign, Illinois, USA.

Niinemets, U. 2001. Global-scale climatic controls of leaf dry mass per area, density, and thickness in trees and shrubs. Ecology 82:453–469.

Niinemets, Ü., T. F. Keenan, and L. Hallik. 2014. A worldwide analysis of within-canopy variations in leaf structural, chemical and physiological traits across plant functional types. New Phytologist.

Ollinger, S. V. 2011. Sources of variability in canopy reflectance and the convergent properties of plants. New Phytologist 189:375–394.

Ollinger, S. V., P. B. Reich, S. Frolking, L. C. Lepine, D. Y. Hollinger, and A. D. Richardson. 2013. Nitrogen cycling, forest canopy reflectance, and emergent properties of ecosystems. Proceedings of the National Academy of Sciences USA 110:E2437–E2437.

Ollinger, S. V., M. L. Smith, M. E. Martin, R. A. Hallett, C. L. Goodale, and J. D. Aber. 2002. Regional variation in foliar chemistry and N cycling among forests of diverse history and composition. Ecology 83:339–355.

Petisco, C., B. Garcia-Criado, S. Mediavilla, B. R. V. de Aldana, I. Zabalgogeazcoa, and A. Garcia-Ciudad. 2006. Near-infrared reflectance spectroscopy as a fast and non-destructive tool to predict foliar organic constituents of several woody species. Analytical and Bioanalytical Chemistry 386:1823–1833.

PRISM. 2004. PRISM Climate Group. Oregon State University. Northwest Alliance for Computational Science and Engineering, Corvallis, Oregon, USA. http://www.prism.oregonstate.edu/

Quested, H., O. Eriksson, C. Fortunel, and E. Garnier. 2007. Plant traits relate to whole-community litter quality and decomposition following land use change. Functional Ecology 21:1016–1026.

Reich, P. B., D. S. Ellsworth, and M. B. Walters. 1998. Leaf structure (specific leaf area) modulates photosynthesis–nitrogen relations: evidence from within and across species and functional groups. Functional Ecology 12:948–958.

Reich, P. B., D. S. Ellsworth, M. B. Walters, J. M. Vose, C. Gresham, J. C. Volin, and W. D. Bowman. 1999. Generality of leaf trait relationships: a test across six biomes. Ecology 80:1955–1969.

Reich, P. B., C. Uhl, M. B. Walters, and D. S. Ellsworth. 1991. Leaf life-span as a determinant of leaf structure and function among 23 Amazonian tree species. Oecologia 86:16–24.

Reich, P. B., M. B. Walters, and D. S. Ellsworth. 1992. Leaf life-span in relation to leaf, plant, and stand characteristics among diverse ecosystems. Ecological Monographs 62:365–392.

Reich, P. B., M. B. Walters, and D. S. Ellsworth. 1997. From tropics to tundra: global convergence in plant functioning. Proceedings of the National Academy of Sciences USA 94:13730–13734.

Reich, P. B., I. J. Wright, J. Cavender-Bares, J. M. Craine, J. Oleksyn, M. Westoby, and M. B. Walters. 2003. The evolution of plant functional variation: traits, spectra, and strategies. International Journal of Plant Sciences 164:S143–S164.

Richardson, A. D., and J. B. Reeves. 2005. Quantitative reflectance spectroscopy as an alternative to traditional wet lab analysis of foliar chemistry: near-infrared and mid-infrared calibrations compared. Canadian Journal of Forest Research 35:1122–1130.

Ripullone, F., G. Grassi, M. Lauteri, and M. Borghetti. 2003. Photosynthesis–nitrogen relationships: interpretation of different patterns between *Pseudotsuga menziesii* and *Populus* × *euroamericana* in a mini-stand experiment. Tree Physiology 23:137–144.

Robinson, D. 2001. δN^{15} as an integrator of the nitrogen cycle. Trends in Ecology and Evolution 16:153–162.

Roujean, J. L., M. Leroy, and P. Y. Deschamps. 1992. A bidirectional reflectance model of the earth's surface for the correction of remote sensing data. Journal of Geophysical Research 97:20455–20468.

Sanchez-Azofeifa, G. A., K. Castro, S. J. Wright, J. Gamon, M. Kalacska, B. Rivard, S. A. Schnitzer, and J. L. Feng. 2009. Differences in leaf traits, leaf internal structure, and spectral reflectance between two communities of lianas and trees: implications for remote sensing in tropical environments. Remote Sensing of Environment 113:2076–2088.

Santiago, L. S. 2007. Extending the leaf economics spectrum to decomposition: evidence from a tropical forest. Ecology 88:1126–1131.

Santiago, L. S., K. Kitajima, S. J. Wright, and S. S. Mulkey. 2004. Coordinated changes in photosynthesis, water relations and leaf nutritional traits of canopy trees along a precipitation gradient in lowland tropical forest. Oecologia 139:495–502.

Schimel, D. S. 1995. Terrestrial ecosystems and the carbon cycle. Global Change Biology 1:77–91.

Scott, N. A., and D. Binkley. 1997. Foliage litter quality and annual net N mineralization: comparison across North American forest sites. Oecologia 111:151–159.

Serbin, S. P., D. N. Dillaway, E. L. Kruger, and P. A. Townsend. 2012. Leaf optical properties reflect variation in photosynthetic metabolism and its sensitivity to temperature. Journal of Experimental Botany 63:489–502.

Serbin, S. P., A. Singh, B. E. McNeil, C. C. Kingdon, and P. A. Townsend. 2014. Spectroscopic determination of leaf morphological and biochemical traits for northern temperate and boreal tree species. Ecological Applications 24:1651–1669.

Serrano, L., J. Penuelas, and S. L. Ustin. 2002. Remote sensing of nitrogen and lignin in Mediterranean vegetation from AVIRIS data: decomposing biochemical from structural signals. Remote Sensing of Environment 81:355–364.

Shipley, B., and M. J. Lechowicz. 2000. The functional co-ordination of leaf morphology, nitrogen concentration, and gas exchange in 40 wetland species. Ecoscience 7:183–194.

Shipley, B., M. J. Lechowicz, I. Wright, and P. B. Reich. 2006. Fundamental trade-offs generating the worldwide leaf economics spectrum. Ecology 87:535–541.

Shipley, B., D. Vile, E. Garnier, I. J. Wright, and H. Poorter. 2005. Functional linkages between leaf traits and net photosynthetic rate: reconciling empirical and mechanistic models. Functional Ecology 19:602–615.

Sims, D. A., and J. A. Gamon. 2002. Relationships between leaf pigment content and spectral reflectance across a wide range of species, leaf structures and developmental stages. Remote Sensing of Environment 81:337–354.

Sims, N. C., D. Culvenor, G. Newnham, N. C. Coops, and P. Hopmans. 2013. Towards the operational use of satellite hyperspectral image data for mapping nutrient status and fertilizer requirements in Australian plantation forests. IEEE Journal of Selected Topics in Applied Earth Observations and Remote Sensing 6:320–328.

Slaton, M. R., E. R. Hunt, and W. K. Smith. 2001. Estimating near-infrared leaf reflectance from leaf structural characteristics. American Journal of Botany 88:278–284.

Smith, M. L., M. E. Martin, L. Plourde, and S. V. Ollinger. 2003. Analysis of hyperspectral data for estimation of temperate forest canopy nitrogen concentration: comparison between an airborne (AVIRIS) and a spaceborne (Hyperion) sensor. IEEE Transactions on Geoscience and Remote Sensing 41:1332–1337.

Soenen, S. A., D. R. Peddle, and C. A. Coburn. 2005. SCS+C: A modified sun-canopy-sensor topographic correction in forested terrain. IEEE Transactions on Geoscience and Remote Sensing 43:2148–2159.

Stuffler, T., et al. 2007. The EnMAP hyperspectral imager: An advanced optical payload for future applications in Earth observation programmes. Acta Astronautica 61:115–120.

Sullivan, F. B., S. V. Ollinger, M. E. Martin, M. J. Ducey, L. C. Lepine, and H. F. Wicklein. 2013. Foliar nitrogen in relation to plant traits and reflectance properties of New Hampshire forests. Canadian Journal of Forest Research 43:18–27.

Tibshirani, R. 1996. Regression shrinkage and selection via the Lasso. Journal of the Royal Statistical Society B 58:267–288.

Townsend, A. R., G. P. Asner, and C. C. Cleveland. 2008. The biogeochemical heterogeneity of tropical forests. Trends in Ecology and Evolution 23:424–431.

Townsend, P. A., J. R. Foster, R. A. Chastain, and W. S. Currie. 2003. Application of imaging spectroscopy to mapping canopy nitrogen in the forests of the central Appalachian Mountains using Hyperion and AVIRIS. IEEE Transactions on Geoscience and Remote Sensing 41:1347–1354.

Townsend, P. A., S. P. Serbin, E. L. Kruger, and J. A. Gamon. 2013. Disentangling the contribution of biological and physical properties of leaves and canopies in imaging spectroscopy data. Proceedings of the National Academy of Sciences USA 110:E1074–E1074.

Tucker, C. J. 1980. Remote-sensing of leaf water-content in the near-infrared. Remote Sensing of Environment 10:23–32.

Ustin, S. L., and J. A. Gamon. 2010. Remote sensing of plant functional types. New Phytologist 186:795–816.

Ustin, S. L., D. Riano, and E. R. Hunt. 2012. Estimating canopy water content from spectroscopy. Israel Journal of Plant Sciences 60:9–23.

Vane, G., R. O. Green, T. G. Chrien, H. T. Enmark, E. G. Hansen, and W. M. Porter. 1993. The Airborne Visible Infrared Imaging Spectrometer (AVIRIS). Remote Sensing of Environment 44:127–143.

Violle, C., E. Garnier, J. Lecoeur, C. Roumet, C. Podeur, A. Blanchard, and M. L. Navas. 2009. Competition, traits and resource depletion in plant communities. Oecologia 160:747–755.

Violle, C., P. B. Reich, S. W. Pacala, B. J. Enquist, and J. Kattge. 2014. The emergence and promise of functional biogeography. Proceedings of the National Academy of Sciences USA 111:13690–13696.

Wessman, C. A., J. D. Aber, and D. L. Peterson. 1989. An evaluation of imaging spectrometry for estimating forest canopy chemistry. International Journal of Remote Sensing 10:1293–1316.

Wold, S. 1994. PLS for multivariate linear modeling. Page 359 in H. Waterbeemd, H. Timmerman, R. Mannhold, and P. Kroqsgaard-Larsen, editors. QSAR: Chemometric methods in molecular design. methods and principles in medicinal chemistry. Wiley, New York, New York, USA.

Wold, S., A. Ruhe, H. Wold, and W. J. Dunn. 1984. The collinearity problem in linear regression: the partial least-squares (PLS) approach to generalized inverses. Siam Journal on Scientific and Statistical Computing 5:735–743.

Wold, S., M. Sjostrom, and L. Eriksson. 2001. PLS-regression: a basic tool of chemometrics. Chemometrics and Intelligent Laboratory Systems 58:109–130.

Wolter, P. T., P. A. Townsend, B. R. Sturtevant, and C. C. Kingdon. 2008. Remote sensing of the distribution and abundance of host species for spruce budworm in Northern Minnesota and Ontario. Remote Sensing of Environment 112:3971–3982.

Wright, I. J., et al. 2005a. Assessing the generality of global leaf trait relationships. New Phytologist 166:485–496.

Wright, I. J., et al. 2005b. Modulation of leaf economic traits and trait relationships by climate. Global Ecology and Biogeography 14:411–421.

Wright, I. J., P. B. Reich, and M. Westoby. 2001. Strategy shifts in leaf physiology, structure and nutrient content between species of high- and low-rainfall and high- and low-nutrient habitats. Functional Ecology 15:423–434.

Wright, I. J., et al. 2004. The worldwide leaf economics spectrum. Nature 428:821–827.

Wright, I. J., and M. Westoby. 2002. Leaves at low versus high rainfall: coordination of structure, lifespan and physiology. New Phytologist 155:403–416.

Yoder, B. J., and R. E. Pettigrewcrosby. 1995. Predicting nitrogen and chlorophyll content and concentrations from reflectance spectra (400V2500 nm) at leaf and canopy scales. Remote Sensing of Environment 53:199–211.

SUPPLEMENTAL MATERIAL

Ecological Archives